p̄p-annihilation into $\omega\pi^0$, $\omega\eta$ and $\omega\eta'$ at 600, 1200 and 1940 MeV/c

The Crystal Barrel Collaboration

A. Abele[8], B. Adomeit[7], C. Amsler[15], C.A. Baker[5], B.M. Barnett[3], C.J. Batty[5], M. Benayoun[12], A. Berdoz[13], K. Beuchert[2,a], S. Bischoff[8], P. Blüm[8], K. Braune[11], T. Case[1], O. Cramer[11], K.M. Crowe[1], T. Degener[2], M. Doser[6], W. Dünnweber[11], D. Engelhardt[8], M.A. Faessler[11], P. Giarritta[15], R.P. Haddock[10], F.H. Heinsius[1,b], M. Heinzelmann[15], A. Herbstrith[8], M. Herz[3], N.P. Hessey[11], P. Hidas[4], C. Holzhaußen[8], D. Jamnik[11,c], H. Kalinowsky[3], P. Kammel[1], J. Kisiel[6,d], E. Klempt[3], H. Koch[2], M. Kunze[2], U. Kurilla[2], M. Lakata[1], R. Landua[6], H. Matthäy[2], R. McCrady[13], J. Meier[7], C.A. Meyer[13], R. Ouared[6], K. Peters[2], B. Pick[3], M. Ratajczak[2], C. Regenfus[15], W. Röthel[11], R. Seibert[7], S. Spanier[15,e], H. Stöck[2], C. Straßburger[3], U. Strohbusch[7], M. Suffert[14], J.S. Suh[3], U. Thoma[3], M. Tischhäuser[8], I. Uman[11], C. Völcker[11], S. Wallis-Plachner[11], D. Walther[3,f], U. Wiedner[6], K. Wittmack[3]

1 University of California, LBL, Berkeley, CA 94720, USA
2 Universität Bochum, 44788 Bochum, Germany
3 Universität Bonn, 53115 Bonn, Germany
4 Academy of Science, 1525 Budapest, Hungary
5 Rutherford Appleton Laboratory, Chilton, Didcot OX11 0QX, UK
6 CERN, 1211 Genève, Switzerland
7 Universität Hamburg, 22761 Hamburg, Germany
8 Universität Karlsruhe, 76021 Karlsruhe, Germany
9 Queen Mary and Westfield College, London E1 4NS, UK
10 University of California, Los Angeles, CA 90024, USA
11 Universität München, 85748 München, Germany
12 LPNHE Paris VI, VII, 75252 Paris, France
13 Carnegie Mellon University, Pittsburgh, PA 15213, USA
14 Centre de Recherches Nucléaires, 67037 Strasbourg, France
15 Universität Zürich, 8057 Zürich, Switzerland

Abstract. The annihilation channels p̄p→$\omega\pi^0$, $\omega\eta$, $\omega\eta'$ were studied with the Crystal Barrel detector at LEAR at p̄-momenta of 600, 1200, and 1940 MeV/c. In most cases angular distributions were measured which allowed a complete J^P-analysis using the helicity formalism. The contribution of all relevant initial states could be determined. The maximal contributing angular momenta are dependent on the p̄-momentum and range up to $J = 5$.

1 Introduction

This paper reports on the measurement of selected two-body p̄p-annihilation channels performed with the Crystal Barrel (CB) detector at LEAR at p̄-momenta of 600, 1200 and 1940 MeV/c. The aims of the measurements were 2-fold: (1) Determine the angular momenta in the

p̄p-system, which contribute to the annihilation process with increasing p̄-momenta. This information is vital for the analysis of 3-or more body annihilation processes in flight, which contain mesonic or exotic resonances with masses up to 2.3 GeV/c^2. (2) Assess whether such data from CB are analyzeable at all. This is not straightforward because the angular distributions are forward peaked in the Lab-system, where the detector, optimized for at rest annihilations, becomes inefficient for γ-detection. The channels ωX(X= π^0, η, η') (X →$\gamma\gamma$; ω→$\pi^0\gamma$) have been chosen, because they provide three independent observables, the production angle Θ of the ω, the decay angle ϑ of the ω and the angle φ between the ω-direction and the ω-decay plane (Treiman-Yang-angle). This informa-

tion allows a complete partial wave analysis using the helicity formalism and thus provides direct information on the contributing initial p̄p-states.

2 Experimental set-up

The experimental set-up for p̄p-experiments at rest with the CB-detector is described in [1]. The set-up used in flight is very similar, but behind the liquid hydrogen target an additional scintillation counter was installed. It consisted of a 3 mm thick disk of 4 cm diameter, mounted at the end of a cylindrical tube of 15 cm diameter and 2 m length, both of which vetoed antiprotons which did not react in the target or were scattered at small angles. According to calculations about 1% of all antiprotons entering the target were not vetoed and thus were candidates for annihilation events inside the target.

The detector is optimized for p̄p-annihilations at rest, for which the two 12 degree holes along the beam line direction have only a small effect. The situation is different at higher antiproton beam momenta due to the Lorentz-boost along the p̄-axis, so that the fraction of undetected particles increases. However, as we will show, this was not a severe limitation in the p̄-momentum range up to 1.94 GeV/c (maximum LEAR momentum) and allowed the measurement of angular distributions over a sufficiently large range.

3 Data sample

Table 1 shows the data samples taken during the various beam periods. In most cases a "0-prong"-trigger was used, rejecting all events with charged particle hits in the cylindrical proportional chambers. In one case (August 1994) a mixed trigger was used, allowing 0- and 2-prong events. The last column refers to the number of truly 0-prong events in the offline analysis.

4 Event reconstruction

The event reconstruction was done in a similar way to that for annihilations at rest, and is described in [2]. The γ's originating from π^0, η, η' and ω-decays hit one of the CsI-crystals of the electromagnetic spectrometer and give rise to electromagnetic showers extending over about 10 crystals in average. A PED (*P*article *E*nergy *D*eposit) is defined as an area consisting of adjacent crystals with energy deposits higher than a minimum value and containing only one maximum. It is normally attributed to the hit of a single γ, but can also be due to a statistical fluctuation (split off) of the shower. A CLUSTER can contain several PEDS.

In contrast to annihilations at rest, the energy of neutral pions can be so high that both decay γ's merge into one PED, because their opening angle in the lab system can be as small as a few degrees. In order to recognize
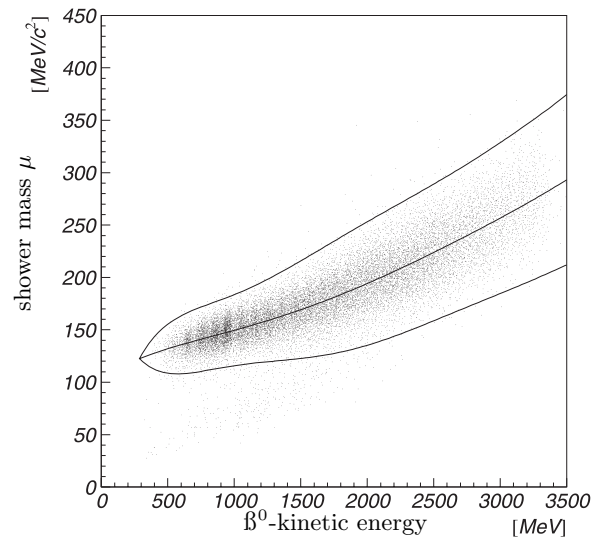

Fig. 1. Monte Carlo-study of the invariant shower mass of two merged γ's from a π^0 as function of π^0 kinetic energy. The inner line corresponds to the center of gravity of the distribution, the outer lines indicate the cut against single γ's

such events, the invariant shower-mass of a PED was determined. It is defined as

$$\mu_{Shower} = \sqrt{\left(\sum_i E_i\right)^2 - \left(\sum_i \overrightarrow{p_i}\right)^2}$$

where i denotes the crystal number, E_i is the γ–energy deposit in crystal i and $\overrightarrow{p_i}$ is the γ–momentum, measured from the annihilation vertex to the crystal i. It has been successfully used in annihilations at rest to distinguish between a shower originating from a single γ and a shower produced by two overlapping γ's [3]. Monte Carlo studies show that the shower masses of single (unmerged) γ's are zero at low momentum rising slowly with energy. The shower masses of merging γ's originating from high energy neutral pions have generally higher values, starting from 140 MeV/c^2 for low energy pions. Both distributions are rather distinct allowing a good separation of events (Fig. 1).

Monte Carlo (MC)-studies showed, that in the reactions discussed here, η and η' cannot produce 1-PED-events, since their decay γ's can always be spatially resolved.

In some cases, π^0's and η's heading towards the forward opening of the detector will escape entirely undetected. In principle, such events could be identified by their missing total energy and momentum, and the remainder of the event could be used to reconstruct the complete event, e.g. by kinematic fitting. As will be apparent from the following and as was confirmed by MC-simulations, these events play only a minor role in the data discussed here. Therefore only complete events fulfilling energy and momentum conservation were used in this analysis.

Table 1. Data sample

beam momentum [MeV/c]	beam period	trigger	total number of events	number of neutral events
600	April/May 1993	0 prong	2 801 862	2 266 054
1200	December 1991	0 prong	1 574 307	1 502 350
	July 1992	0 prong	1 409 025	1 321 896
	April/May 1993	0 prong	8 690 455	7 315 274
	August 1994	0 prong	1 414 995	1 081 728
		Σ	13 088 782	11 221 048
1940	July 1992	0 prong	6 945 965	5 590 895
	August 1994	0 prong	3 263 167	2 527 387
	August 1994	mixed		440 695
		Σ		8 558 977

Table 2. Steps of data selection for the $0^-\omega$ channels. Detailed explanations are given in the text

|	beam momentum [MeV/c]	600	1200	1940
	# of neutral events	2 266 054	10 923 847	8 558 977
general selection	cuts on multiplicities			
	1. PED-multiplicity ($4 \leq \#_{\text{PEDs}} \leq 10$)	1 608 966	8 431 557	6 044 919
	2. Removal of split offs	1 603 230	8 315 659	5 916 326
	3. Max. # of π^0 and η	250 224	1 222 317	839 153
	kinematic fit			
	4. final state (5γ or $\pi^0\gamma\gamma\gamma$)	75 121	381 910	181 858
	5. $\pi^0 X\gamma$ (X = π^0, η or η')	59 146	327 784	160 049
	6. $\omega\gamma\gamma$	33 515	170 466	73 710
	7. vertex	31 920	163 245	63 790
channel specific selection	8. $\bar{p}p \longrightarrow \pi^0\omega$			
	a. consistency of $\pi^0\pi^0\gamma$ and $\omega\gamma\gamma$	12 486	64 716	28 485
	b. consistency with meson recognition	12 462	64 340	27 989
	c. no shower fluctuation (5 PEDs at most)	8 183	41 663	17 320
	9. $\bar{p}p \longrightarrow \eta\omega$			
	a. consistency of $\pi^0\eta\gamma$ and $\omega\gamma\gamma$	5 421	20 029	7 051
	b. consistency of meson recognition	4 875	17 667	6 102
	c. no shower fluctuation (5 PEDs at most)	3 269	11 283	3 660
	d. no merged π^0 ("1-PED-π^0")	3 269	11 222	3 434
	e. cut on ω decay angle	2 880	9 732	3 032
	10. $\bar{p}p \longrightarrow \eta'\omega$			
	a. consistency of $\pi^0\eta'\gamma$ and $\omega\gamma\gamma$	1 964	too low statistics	
	b. consistency with meson recognition	670	with too large	
	c. no shower fluctuation (5 PEDs at most)	393	background	
	d. no merged π^0 ("1-PED-π^0")	393		
	survey of selected statistics			
	$\bar{p}p \longrightarrow \pi^0\omega$ (4 & 5 PEDs)	8 183	41 663	17 320
	5 PEDs	8 181	40 898	14 263
	4 PEDs	2	765	3 057
	$\bar{p}p \longrightarrow \eta\omega$ (5 PEDs)	2 880	9 732	3 032
	$\bar{p}p \longrightarrow \eta'\omega$ (5 PEDs)	393	too low statistics	
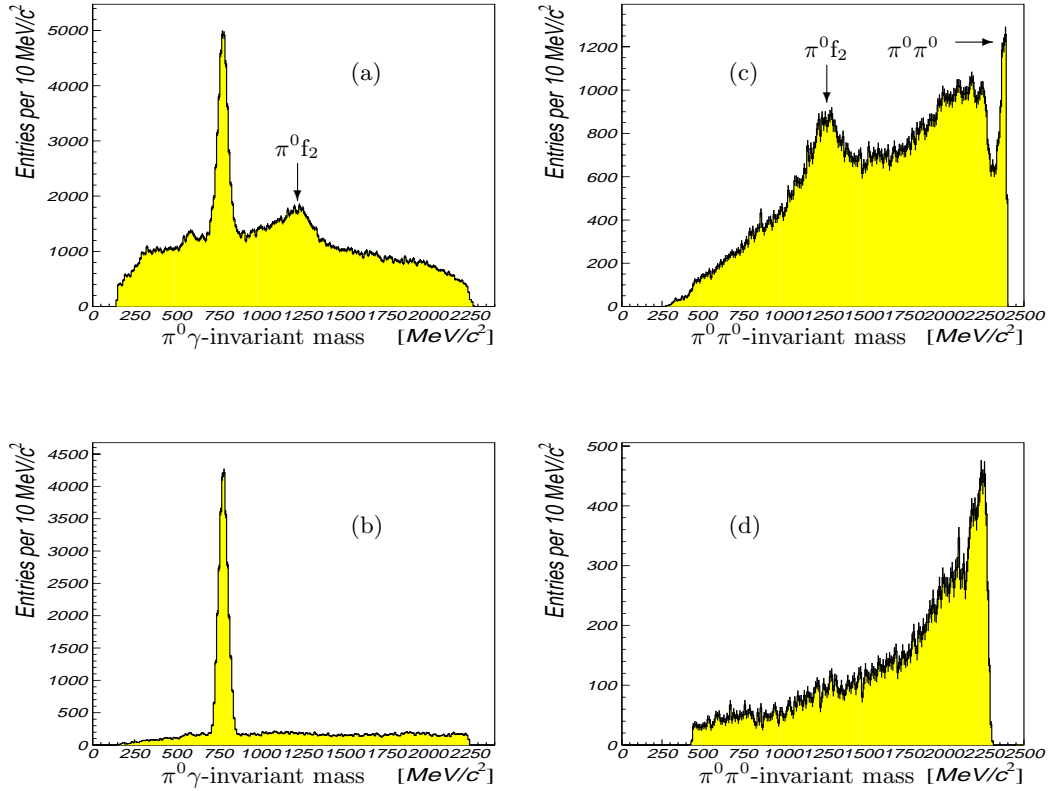
Fig. 2a–d. Control spectra for the $\pi^0\omega$ selection at 1940 MeV/c. **a,b** show the invariant mass spectra of $\pi^0\gamma$ (2 entries per event), Figs. 2c,d show the invariant mass spectra of $\pi^0\pi^0$ (1 entry per event). **a,c** give the spectra after the $\pi^0\pi^0\gamma$ fit (step 5). **b,d** refer to the spectra after step 8a

Table 2 shows the steps in the data reconstruction and the applied cuts to reduce the instrumental background (e.g. electronic noise) and the physical background (e.g. shower fluctuations or punchthroughs of high multiplicity channels). The first line gives the number of neutral events at the three p̄-momenta investigated. "Neutral" means, that there was no hit in either of the two cylindrical proportional wire chambers nor in the inner three layers of the jet-drift-chamber . Step 1 lists the number of events after a cut on the number of PEDS. The minimum value (4) corresponds to one 1-PED π^0 +3 γ as it never occurs that both π^0's of an event form a single PED, the maximum value (10) corresponds to 5 γ PEDS + 5 split-offs. The next cut (step 2) tries to separate single γ PEDS from split offs. This is done using the neural network "Brain" [4], which was extensively checked with MC-data. In the next cut (step 3), events are restricted to those with maximally two π^0's or one π^0 and one η.

The events with one 1 PED π^0+ three γ's and those with five γ's were kinematically fitted to the hypothesis 5 γ or $\pi^0\gamma\gamma\gamma$ (step 4), and then to the hypothesis $\pi^0 X\gamma(X=\pi^0, \eta, \eta')$ (step 5) and $\omega\gamma\gamma$ (step 6). Figs. 2a/c show the $\pi^0\gamma$-and $\pi^0\pi^0$-invariant masses for the $\pi^0\omega$-channel after step 5. It is obvious, that background, e.g. from $\pi^0 f_2$ ($f_2\rightarrow\pi^0\pi^0$, one γ missing), 3 π^0 (one γ missing) and $2\pi^0$(+ one splitoff) is still present. In order to

reduce this background a cut on the vertex distribution was applied. In the absence of charged annihilation products, the vertex could be determined only crudely by a kinematic fit to the events. This cut removed events originating from the veto counter behind the target (step 7).

Further cuts were channel specific. As an example, the $\pi^0\omega$-channel is discussed in more details. As no direct fit to the channel $\pi^0\omega$ was done due to the width of the ω and in order to keep control on background a consistency check between the hypotheses of step 5 and 6 was made. Only those events were kept for which either of the two γ's of the $\omega\gamma\gamma$-hypothesis did not coincide with the γ of the $\pi^0\pi^0\gamma$-hypothesis (step 8a). This gave a huge reduction of the background in the $\pi^0\gamma$- and $\pi^0\pi^0$- invariant mass spectra (Figs. 2b/d). Furthermore the assignment of π^0, η and η' particles to two γ's was checked by comparing the identification methods used in step 3 (invariant $\gamma\gamma$-masses) and step 5, which are independent. Consistency between the two methods was required (step 8b).

Comparing the backgrounds in the data with MC-predictions we found it to be too large for some subsamples of the data. This was particularly true for events where split-offs had been recognized by "Brain", so that these events were finally removed (step 8c).

A similar procedure was applied for the selection of the $\eta\omega$-channel(see steps 9a-e). Here two further cuts were

600 MeV/c 1200 MeV/c 1940 MeV/c

ω-production angle
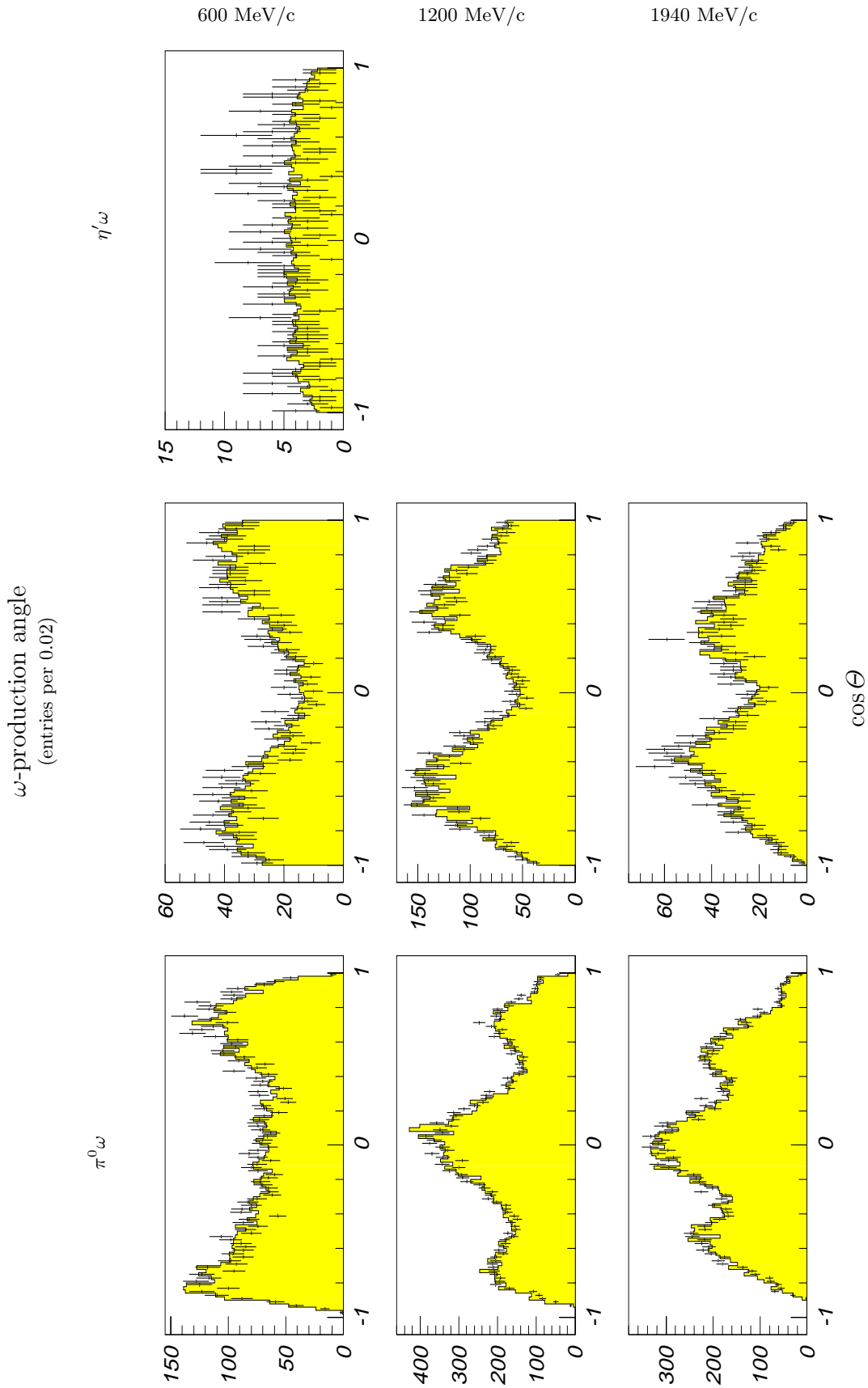(entries per 0.02)

Fig. 3. Distributions of the ω production angle Θ (not corrected for acceptance). The points with the error bars correspond to the data, the fit results are given as shaded areas

Fig. 4. Distributions of the ω decay angle θ and the Treiman Yang angle φ (not corrected for acceptance). The points with the error bars correspond to the data, the fit results are given as shaded areas

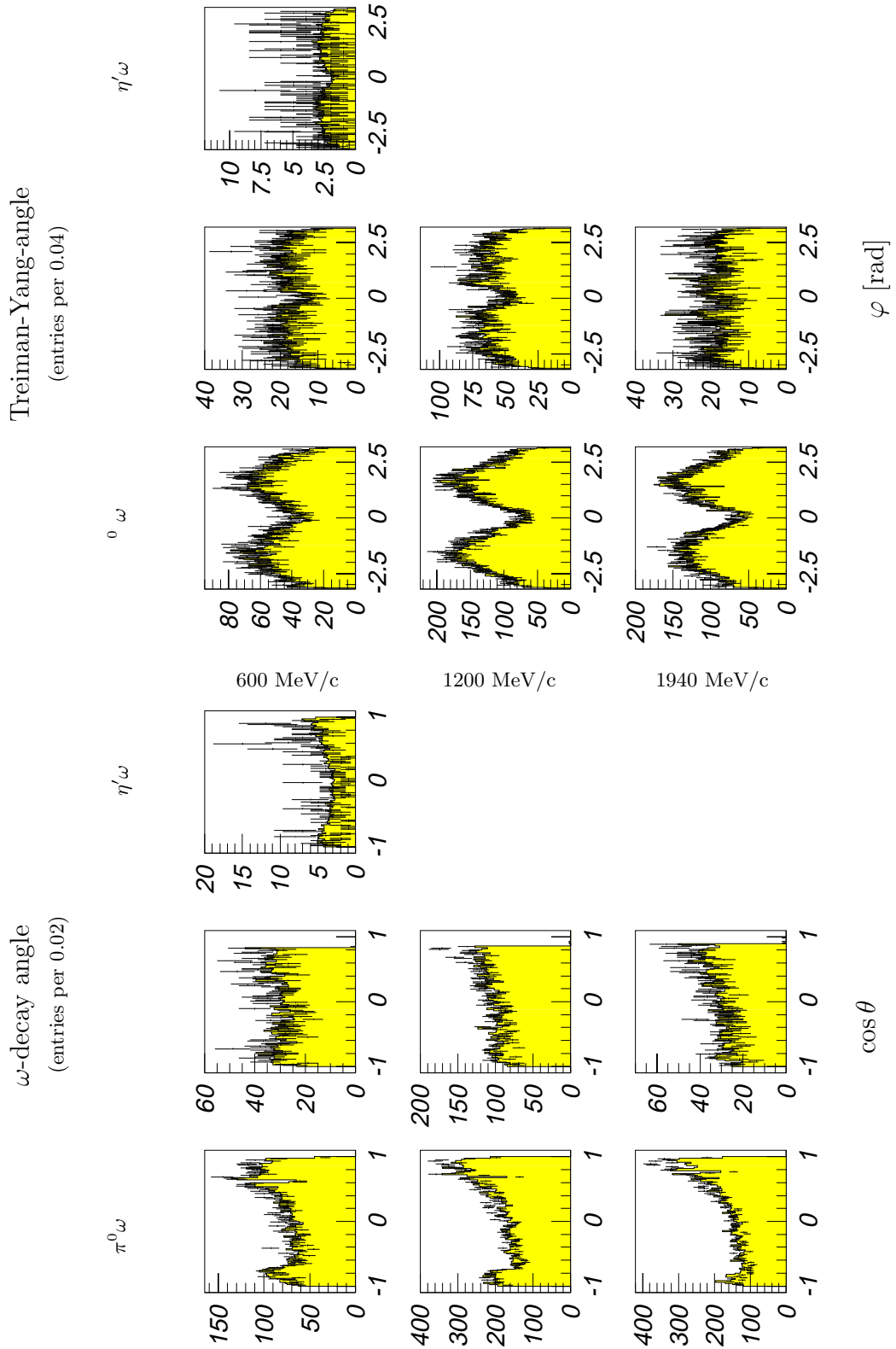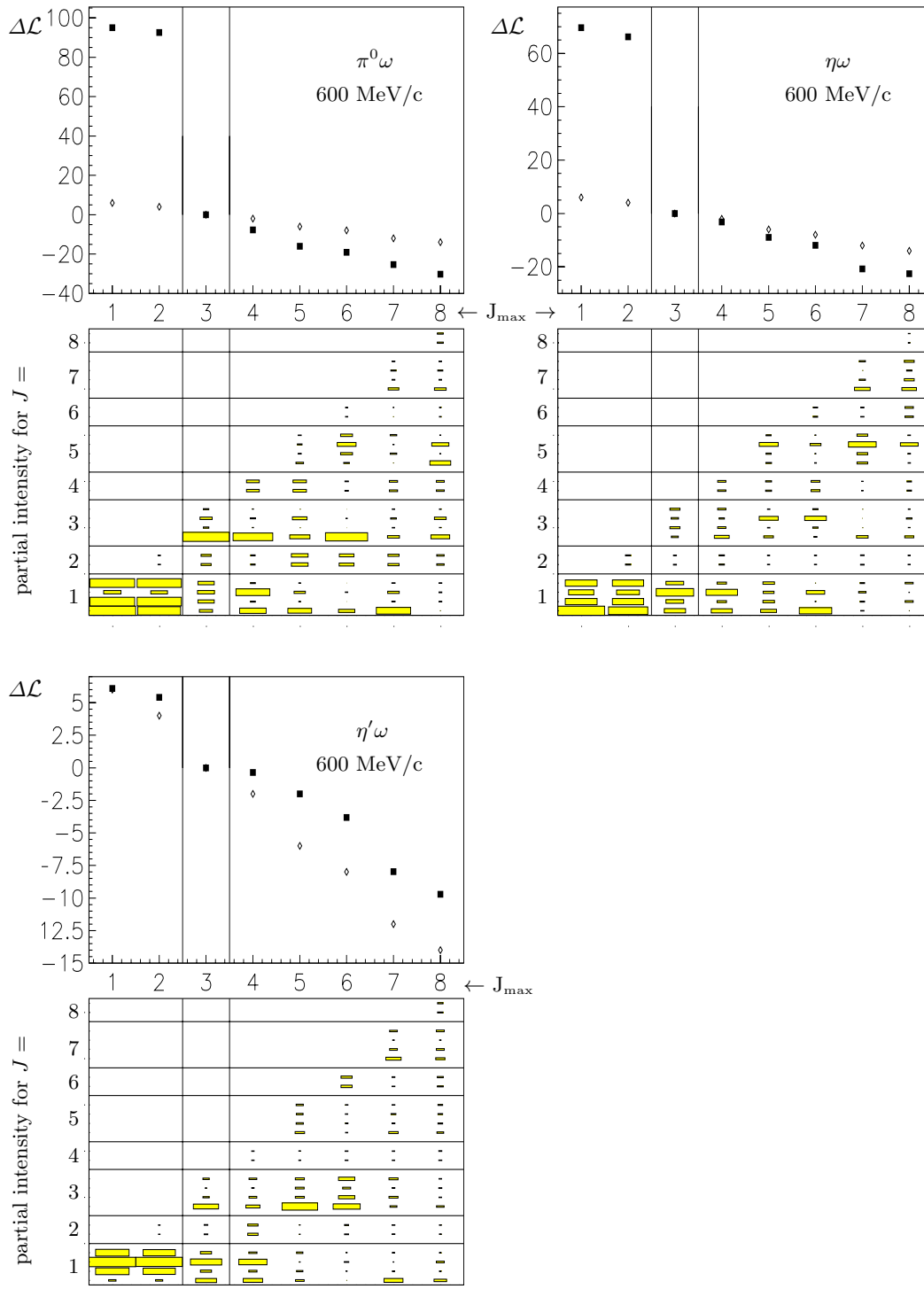**Fig. 5.** Upper figures: Change of Log-likelihood values $\Delta\mathcal{L}$ (black squares) as a function of J_{max} as fitted to the data. The open diamonds describe the expected change of $\Delta\mathcal{L}$ only due to the increase of the number of degrees of freedom (see text) Lower figures: Partial intensities for different J–values as a function of J_{max}. From bottom to top: singlet $M = 0$, triplet $M = -1, 0, +1$ for J odd, and triplet $M = -1, +1$ for J even. The value J_{max}^{contr} is emphasized by vertical lines

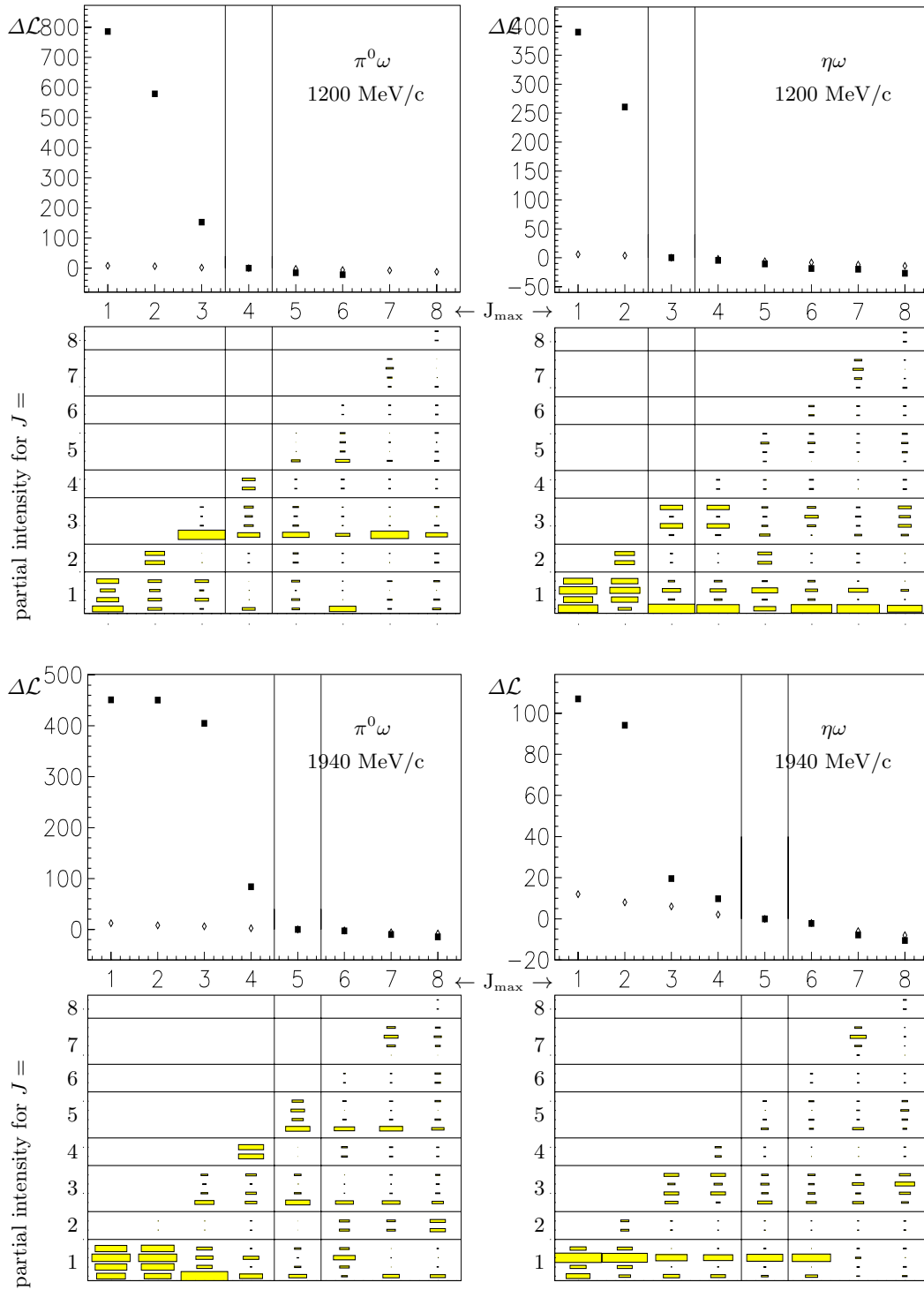**Fig. 6.** Change of Log-likelihood values $\Delta\mathcal{L}$ and the Partial intensities for 1200 and 1940 MeV/c. For explanation of symbols see Fig. 5

Table 3. Magnitudes and phases of α_L^{JM}, describing the best fit to the angular distributions for the case $J_{max} = J_{max}^{contr}$. The beam momentum is 600 MeV/c

channel	J^{PC}	M	L	$|\alpha_L^{JM}|$	φ_L^{JM}
$\pi^0\omega$	1^{--}	0	1	0.41 ± 0.19	0. (fixed)
600 MeV/c		± 1	1	0.40 ± 0.17	0. (fixed)
	1^{+-}	0	0	0.17 ± 0.07	0. (fixed)
			2	0.26 ± 0.13	0.70 ± 0.27
	2^{--}	± 1	1	0.25 ± 0.12	2.49 ± 0.23
			3	0.31 ± 0.11	5.66 ± 0.25
	3^{--}	0	3	0.53 ± 0.21	-1.05 ± 0.18
		± 1	3	0.36 ± 0.16	2.06 ± 0.26
	3^{+-}	0	2	0.77 ± 0.27	-1.32 ± 0.15
			4	0.57 ± 0.22	-0.20 ± 0.17
$\eta\omega$	1^{--}	0	1	0.66 ± 0.34	0. (fixed)
600 MeV/c		± 1	1	0.45 ± 0.31	0. (fixed)
	1^{+-}	0	0	0.23 ± 0.22	0. (fixed)
			2	0.37 ± 0.25	-5.60 ± 1.57
	2^{--}	± 1	1	0.11 ± 0.13	-0.73 ± 0.66
			3	0.24 ± 0.19	-4.17 ± 0.59
	3^{--}	0	3	0.45 ± 0.24	3.14 ± 2.47
		± 1	3	0.52 ± 0.28	-4.81 ± 0.38
	3^{+-}	0	2	0.32 ± 0.27	-4.70 ± 0.49
			4	0.23 ± 0.21	-5.75 ± 0.79
$\eta'\omega$	1^{--}	0	1	0.61 ± 0.48	0. (fixed)
600 MeV/c		± 1	1	0.36 ± 0.35	0. (fixed)
	1^{+-}	0	0	0.23 ± 0.21	0. (fixed)
			2	0.37 ± 0.33	0.49 ± 0.66
	2^{--}	± 1	1	0.17 ± 0.20	-0.99 ± 0.99
			3	0.19 ± 0.25	-0.78 ± 1.08
	3^{--}	0	3	0.22 ± 0.41	-3.14 ± 2.77
		± 1	3	0.42 ± 0.41	2.27 ± 0.67
	3^{+-}	0	2	0.65 ± 0.50	1.33 ± 0.46
			4	0.40 ± 0.35	0.55 ± 0.71

Table 4. Magnitudes and phases of α_L^{JM}, describing the best fit to the angular distributions for the case $J_{max} = J_{max}^{contr}$. The beam momentum is 1200 MeV/c

channel	J^{PC}	M	L	$|\alpha_L^{JM}|$	φ_L^{JM}
$\pi^0\omega$	1^{--}	0	1	0.52 ± 0.04	0. (fixed)
1200 MeV/c		± 1	1	0.02 ± 0.06	0. (fixed)
	1^{+-}	0	0	0.22 ± 0.04	0. (fixed)
			2	0.32 ± 0.09	0.12 ± 0.12
	2^{--}	± 1	1	0.11 ± 0.03	1.24 ± 0.33
			3	0.17 ± 0.05	0.81 ± 0.29
	3^{--}	0	3	0.53 ± 0.10	-3.15 ± 6.28
		± 1	3	0.59 ± 0.10	-1.82 ± 0.21
	3^{+-}	0	2	0.78 ± 0.15	-4.24 ± 0.10
			4	0.06 ± 0.05	1.72 ± 1.25
	4^{--}	± 1	3	0.51 ± 0.10	-1.90 ± 0.21
			5	0.58 ± 0.11	4.57 ± 0.21
$\eta\omega$	1^{--}	0	1	0.46 ± 0.09	0. (fixed)
1200 MeV/c		± 1	1	0.27 ± 0.08	0. (fixed)
	1^{+-}	0	0	0.39 ± 0.08	0. (fixed)
			2	0.33 ± 0.08	5.62 ± 0.31
	2^{--}	± 1	1	0.10 ± 0.18	0.45 ± 0.29
			3	0.19 ± 0.10	3.42 ± 0.34
	3^{--}	0	3	0.32 ± 0.08	0.00 ± 1.57
		± 1	3	0.77 ± 0.15	0.69 ± 0.37
	3^{+-}	0	2	0.22 ± 0.23	4.93 ± 0.54
			4	0.26 ± 0.22	4.44 ± 0.18

applied. A comparison between data (after step 9c) and MC-predictions showed too large a background for the 1-PED-π^0-events. Consequently these events were skipped (step 9d). Furthermore, the inspection of the ω-decay angular distribution showed an accumulation of events near $\cos\theta = 1$. According to MC-calculations it originated from falsely identified $\pi^0\omega$-events and so events with $\cos\theta > 0.84(600MeV/c), 0.86(1200MeV/c)$ and $0.90(1940MeV/c)$ were cut off (step 9e).

The $\eta'\omega$-channel was treated similarly, but no cut on $\cos\theta$ was necessary. The data were reconstructed only for 600 MeV/c p̄-momentum as the background at higher p̄-momenta was too big. This is due to the fact that η' was analysed in its 2γ decay mode only, which has a low branching ratio (2.1 %).

The resulting angular distributions for the three two body channels and the three momenta under investigation are shown in Fig. 3 and Fig. 4.

5 Background estimate

MC–data for the channels $\pi^0\omega$, $\eta\omega$, $\eta'\omega$, $\pi^0\pi^0$, $\pi^0\eta$, $\pi^0\eta'$, $\eta\eta$, $3\pi^0$, $2\pi^0\eta$ and $3\,\eta$ were produced at the p̄-momenta under investigation. For the 2–body channels the angular distributions found here and from [5] were used and corrected for acceptance. For the simulation of 3–body channels at 600 and 1940 MeV/c no intermediate resonances were taken into account. However, it was found in MC-studies that the inclusion of intermediate states as found in [6] even reduces the feed through into the ωX-channels. The background contributions could be determined by processing these data through the analysis chain discussed above. For the $\pi^0\omega$-channel they varied between 5% (600 MeV/c) and 13 % (1940 MeV/c) (main contribution from $3\,\pi^0$), for the $\eta\omega$-channel between 4% and 14% (main contribution from $\pi^0\omega$, $3\pi^0$ and $2\pi^0\eta$), while for the $\eta'\omega$-channel (600 MeV/c) the background is as high as 21 %, mainly from $\pi^0\omega$, $\eta\omega$, $3\pi^0$ and $2\pi^0\eta$.

6 Partial wave analysis

For the partial wave analysis it is assumed that the initial states are well defined p̄p–states with quantum numbers J^{PC}. The direction of the incoming p̄ is chosen as the quantization axis, so that the third component of J is

Table 5. Magnitudes and phases of α_L^{JM}, describing the best fit to the angular distributions for the case $J_{max} = J_{max}^{contr}$. The beam momentum is 1940 MeV/c

channel	J^{PC}	M	L	$|\alpha_L^{JM}|$	φ_L^{JM}
$\pi^0\omega$	1^{--}	0	1	0.14 ± 0.08	0. (fixed)
1940 MeV/c		± 1	1	0.27 ± 0.04	0. (fixed)
	1^{+-}	0	0	0.26 ± 0.02	0. (fixed)
			2	0.09 ± 0.04	-1.17 ± 0.29
	2^{--}	± 1	1	0.01 ± 0.02	5.60 ± 3.00
			3	0.05 ± 0.04	-0.06 ± 0.62
	3^{--}	0	3	0.03 ± 0.06	0.00 ± 6.28
		± 1	3	0.42 ± 0.07	2.38 ± 0.08
	3^{+-}	0	2	0.59 ± 0.04	1.19 ± 0.08
			4	0.47 ± 0.06	-4.35 ± 0.09
	4^{--}	± 1	3	0.04 ± 0.06	0.88 ± 1.36
			5	0.05 ± 0.06	2.76 ± 1.00
	5^{--}	0	5	0.76 ± 0.07	-3.14 ± 4.58
		± 1	5	0.69 ± 0.04	0.58 ± 0.07
	5^{+-}	0	4	0.54 ± 0.04	4.36 ± 0.10
			6	0.89 ± 0.05	3.89 ± 0.07
$\eta\omega$	1^{--}	0	1	0.74 ± 0.03	0. (fixed)
1940 MeV/c		± 1	1	0.18 ± 0.02	0. (fixed)
	1^{+-}	0	0	0.18 ± 0.01	0. (fixed)
			2	0.08 ± 0.04	-3.96 ± 0.39
	2^{--}	± 1	1	0.04 ± 0.01	0.25 ± 0.68
			3	0.17 ± 0.02	1.74 ± 0.12
	3^{--}	0	3	0.54 ± 0.03	5.43 ± 0.08
		± 1	3	0.48 ± 0.04	5.18 ± 0.07
	3^{+-}	0	2	0.60 ± 0.02	0.84 ± 0.04
			4	0.03 ± 0.02	-0.04 ± 1.10
	4^{--}	± 1	3	0.04 ± 0.03	-0.52 ± 0.74
			5	0.32 ± 0.04	-1.12 ± 0.08
	5^{--}	0	5	0.00 ± 0.26	3.05 ± 0.00
		± 1	5	0.45 ± 0.02	1.88 ± 0.09
	5^{+-}	0	4	0.31 ± 0.02	3.16 ± 0.09
			6	0.58 ± 0.04	-4.11 ± 0.04

restricted to $M = 0, \pm 1$. The $0^-\omega$–system is characterized by the quantum numbers L (angular momentum), total spin S (=1), total helicity Λ (= ω-helicity) and the decay angles Θ and Φ of the ω-direction. The $\omega \to \pi^0\gamma$–system is characterized by the angular momentum ℓ (=1), total spin s (=1), the total helicity λ (= γ-helicity) and the decay angles θ and φ. s_ω, λ_ω and s_γ, λ_γ are the spins and helicities of the ω and γ, respectively.

The quantities which the analysis aims to determine are the frequencies with which the initial states of different J and M-values contribute to the measured angular distributions. Taking into account the conservation of parity (P), charge conjugation (C), total angular momentum (J) and of its z–component (M), it turns out, that only specific J^{PC} and M-values are allowed for the process

$\bar{p}p \to 0^-\omega$. $J = 0$ states are excluded. For $J =$ even-states only J^{--} with $M = \pm 1$ is allowed, for $J =$ odd-states only J^{--} with $M = 0, \pm 1$ and J^{+-} with $M = 0$ contribute.

The amplitudes are derived from the formulae given in [7]. Quantities needing coherent summation are written as subscripts and quantities needing incoherent summation are written as superscripts on the amplitudes. Then the amplitude reads:

$$A_{J\lambda_\omega}^{M\lambda_\gamma}(\bar{p}p \to 0^-\omega \to 0^-\pi^0\gamma) = \qquad (1)$$
$$A_{J\lambda_\omega}^{M}(\bar{p}p \to 0^-\omega) \times A_{\lambda_\omega}^{\lambda_\gamma}(\omega \to \pi^0\gamma) =$$
$$\sum_{LS} \alpha_{LS}^{JM}(\bar{p}p) \, (L\,0\,S\,\Lambda \,|\, J\,\Lambda) \, (s_\omega\,\lambda_\omega\,0\,0\,|\,S\,\Lambda) \times$$
$$D_{M\Lambda}^{J}{}^*(\Phi, \Theta, 0) \times$$
$$\sum_{\ell\sigma} \alpha_{\ell s}^{JM}(\omega) \, (\ell\,0\,s\,\lambda\,|\,s_\omega\,\lambda) \, (s_\gamma\,\lambda_\gamma\,0\,0\,|\,\sigma\,\lambda) \times$$
$$D_{\lambda_\omega\lambda}^{1}{}^*(\varphi, \theta, 0)$$

The α_{LS} denote the complex spin orbit coupling amplitudes which are free parameters of the fit. With S = s_ω = 1, s = s_γ = 1 and ℓ = 1 (follows from parity conservation) and setting

$$\sqrt{3}\alpha_{L1}^{JM}(\bar{p}p)\alpha_{11}^{JM}(\omega) = \alpha_L^{JM} = |\alpha_L^{JM}|e^{i\varphi_L^{JM}},$$

one obtains

$$A_{J\lambda_\omega}^{M\lambda_\gamma}(\bar{p}p \to 0^-\omega \to 0^-\pi^0\gamma) = \qquad (2)$$
$$-\sqrt{\pi} \, \lambda_\gamma \, e^{i\lambda_\omega\varphi} \, d_{M\lambda_\omega}^{J}(cos\Theta) \, d_{\lambda_\omega\lambda_\gamma}^{1}(cos\theta) \times$$
$$\sum_L |\alpha_L^{JM}| \, (L\,0\,1\,\lambda_\omega\,|\,J\,\lambda_\omega)e^{i\varphi_L^{JM}}$$

The observed intensity is given as the modulus of (2) with coherent summation over J and λ_ω and incoherent summation over M and λ_γ. This theoretical ansatz was used to describe the data. The magnitudes and phases of α_L^{JM} were the free parameters to be fitted to the data. With α_L^{JM} being equal for $M = +1$ and $M = -1$, three arbitrary phases remained, which were set to zero. The minimization was done using a maximum likelihood method. For every iteration the fit results were treated as the weights to a MC-simulation, assuming an isotropic distribution of the events in the CM-system, thus allowing a detailed fit-data comparison for every step. Figs. 3 and 4 show the results for the best final fits compared to the data. The agreement between fits and data is very good within errors. Tables 3,4,5 give the magnitudes and phases of α_L^{JM}, as obtained from the fit with $J_{max} = J_{max}^{contr}$ (see next section). The errors are purely statistical.

7 Discussion of results and conclusions

In order to obtain the maximal contributing angular momenta $J_{\max}^{contr}$, several fits with successively increasing maximal angular momentum $J_{\max}$ were performed for each

Table 6. Contributing maximal angular momenta for $0^-\omega$, 0^-0^- [5] and $\omega\omega$ [9]

decay channel		$\pi^0\pi^0$	$\pi^0\eta$	$\pi^0\omega$	$\eta\eta$	$\eta\omega$	$\omega\omega$	$\eta'\omega$
mass [MeV/c²]		269.95	682.43	916.92	1094.90	1329.39	1563.88	1739.71
momentum	600 MeV/c	2		3		3		3
	1200 MeV/c	4	4	4	4	3		
	1940 MeV/c	6	6	5	4	5	4	

beam momentum. For each of these fits every allowed transition with an angular momentum $J \leq J_{\max}$ was taken into account. Partial intensities were defined in order to visualize the result of every step. These are intensities calculated for a given angular momentum $J \leq J_{\max}$ and one value of M. Figs. 5 and 6 show the development of these partial intensities for the three channels and the three p̄-momenta under study. For even J values two M values (± 1) are possible, for odd J values a singlet ($M = 0$) and a triplet state ($M = 0, \pm 1$) occur. The partial intensities are displayed as boxes whose size is proportional to their magnitudes. Also shown is the variation of the log likelihood $\Delta\mathcal{L}$ with $J_{\max}$ (black squares). The behaviour of $\Delta\mathcal{L}$ is taken as the criterion for the determination of the maximal contributing angular momentum $J_{\max}^{contr}$. It is observed that after reaching a certain value of $J_{\max}$ the change in the likelihood levels off and comes close to the values displayed by open diamonds in Figs. 5 and 6. They correspond to changes in $\mathcal{L}$ expected for the case that a maximum is found and additional degrees of freedom do not give a refined description of the data. $\mathcal{L}$ is then only diminished due to the higher number of degrees of freedom. A diminination in $\Delta\mathcal{L}$ of 0.5 was assumed per degree of freedom. $J_{\max}^{contr}$ is then defined as the value of $J_{\max}$, for which both curves begin to have the same shape. It is emphasized in the figures by vertical lines. According to this definition the maximum contributing angular momenta are:

- $J_{\max}^{contr} = 5$ for p̄p $\longrightarrow \pi^0\omega$ at 1940 MeV/c
- $J_{\max}^{contr} = 5$ for p̄p $\longrightarrow \eta\omega$ at 1940 MeV/c
- $J_{\max}^{contr} = 4$ for p̄p $\longrightarrow \pi^0\omega$ at 1200 MeV/c
- $J_{\max}^{contr} = 3$ for p̄p $\longrightarrow \eta\omega$ at 1200 MeV/c
- $J_{\max}^{contr} = 3$ for p̄p $\longrightarrow \pi^0\omega$ at 600 MeV/c
- $J_{\max}^{contr} = 3$ for p̄p $\longrightarrow \eta\omega$ at 600 MeV/c
- $J_{\max}^{contr}$ compatible with 3 for p̄p $\longrightarrow \eta'\omega$ at 600 MeV/c

These values are in agreement with estimates of $J_{\max}^{contr}$ as obtained by model calculations (see e.g. [8]).
Some characteristics of the results are:

- even angular momenta are suppressed for all channels at all momenta
- for p̄p $\longrightarrow \pi^0\omega$ (all momenta): The dominant contributions originate from $J = J_{\max}^{contr}$
- for p̄p $\longrightarrow \eta\omega$ (all momenta): The dominant contributions originate from $J < J_{\max}^{contr}$
- $M = 0$ singlet states are preferred for p̄p $\longrightarrow \pi^0\omega$
- $M = 0$ triplet states are preferred for p̄p $\longrightarrow \eta\omega$ (exception: 1200 MeV/c).

It is interesting to consider the dependence of the maximal contributing angular momenta on the produced mass.

Table 6 shows the values of $J_{\max}^{contr}$ for the reactions discussed here. In addition values for two 0^-0^- reactions [5] and for $\omega\omega$–annihilation [9] are given. The columns are arranged from left to right according to the masses of the particles produced. There is a slight tendency for $J_{\max}^{contr}$-values to decrease with increasing masses (e.g. $\pi^0\omega/\eta\omega$ at 1200 MeV/c). The value $J_{\max}^{contr} = 2$ for p̄p $\longrightarrow \pi^0\pi^0$ at 600 MeV/c does not contradict this tendency, because J=3 is not allowed for 0^-0^-–final states.

The data and analyses presented here form the basis for future work on p̄p-annihilations in flight measured with the CB-detector. They demonstrate that the CB-detector in spite of its geometry is able to reasonably measure forward peaked angular distributions. In the meantime, similar data have been taken at further p̄-momenta and are presently being evaluated. Together with the data presented here, they will form a set of data allowing a mass scan of specific partial waves up to 2.4 GeV/c^2.

References

1. E. Aker et al., Nucl. Inst. and Meth. A **321** (1992) 69
2. C. Amsler et al., Z. Phys. C **58** (1993) 175
3. S. Kelzenberg: Diploma thesis, University of Karlsruhe, 1990, unpublished
4. T. Degener: Diploma thesis, University of Bochum, 1993, unpublished
5. K. Beuchert: PhD thesis, University of Bochum, 1996, Publisher: Verlag Bülbül, Bochum
6. A. Abele et al., Observation of resonances in the reaction $\bar{p}p \to \pi^0\eta\eta$ at 1.94 GeV/c, accepted for publication by Euro Phys. Journal C
7. S. U. Chung: Spin formalisms, CERN 71-8, 1971
8. W. Weise: Nucl. Phys. A **558** (1993) 219C
9. V. Credé: Diploma thesis, University of Bochum, 1996, unpublished